Acidity of expiratory aerosols controls the infectivity of airborne influenza virus and SARS-CoV-2

Beiping Luo[1,†], Aline Schaub[2,†], Irina Glas[3,†], Liviana K. Klein[1,†], Shannon C. David[2], Nir Bluvshtein[1], Kalliopi Violaki[4], Ghislain Motos[4], Marie Pohl[3], Walter Hugentobler[4], Athanasios Nenes[4,5], Ulrich K. Krieger[1], Silke Stertz[3], Thomas Peter[1,*], and Tamar Kohn[2,*]

[1]Institute for Atmospheric and Climate Science, ETH Zurich, Zurich, Switzerland
[2]Environmental Chemistry Laboratory, School of Architecture, Civil and Environmental Engineering, Ecole Polytechnique Fédérale de Lausanne (EPFL), Lausanne, Switzerland
[3]Institute of Medical Virology, University of Zurich, Zurich, Switzerland
[4]Laboratory of Atmospheric Processes and their Impacts, School of Architecture, Civil and Environmental Engineering, Ecole Polytechnique Fédérale de Lausanne (EPFL), Lausanne, Switzerland
[5]Institute of Chemical Engineering Sciences, Foundation for Research and Technology Hellas, Patras, Greece
[†]these authors contributed equally to this work
[*]Corresponding authors: tamar.kohn@epfl.ch and thomas.peter@env.ethz.ch

Enveloped viruses are prone to inactivation when exposed to strong acidity levels characteristic of atmospheric aerosol. Yet, the acidity of expiratory aerosol particles and its effect on airborne virus persistence has not been examined. Here, we combine pH-dependent inactivation rates of influenza A virus and SARS-CoV-2 with microphysical properties of respiratory fluids under indoor conditions using a biophysical aerosol model. We find that particles exhaled into indoor air become mildly acidic (pH $\approx$ 4), rapidly inactivating influenza A virus within minutes, whereas SARS-CoV-2 requires days. If indoor air is enriched with non-hazardous levels of nitric acid, aerosol pH drops by up to 2 units, decreasing 99%-inactivation times for both viruses in small aerosol particles to below 30 seconds.Conversely, unintentional removal of volatile acids from indoor air by filtration may elevate pH and prolong airborne virus persistence. The overlooked role of aerosol pH has profound implications for virus transmission and mitigation strategies.

One Sentence Summary: Respiratory viruses are sensitive to aerosol pH, an unidentified factor in the mitigation of airborne virus transmission

Respiratory viral infections pose a great burden on human health. An average of 400 000 deaths are associated with influenza globally each year (*1*), and the ongoing COVID-19 pandemic has already resulted in several million deaths and countless cases of long COVID around the world. To curb the public health and economic impacts of these diseases, health care policy aims to minimize virus transmission. Increasing evidence points to expiratory aerosol particles (see (*2*) for clarification of terminology) as vehicles for the transmission of influenza virus and SARS-CoV-2 (*3*). The persistence of these viruses in aerosols is still subject to scientific debate, but it is undisputed that rapid inactivation would contribute to limiting their spread.

Prior studies have investigated the effect of ambient conditions on the inactivation rates of aerosolized respiratory viruses including influenza virus (*4, 5, 6, 7, 8, 9*), SARS-CoV-2 (*10, 11, 12*), and the common cold human coronavirus HCoV-229E (*13*). Relative humidity (RH) and temperature were the primary variables modulated in these works, with low ($\sim$ 20%), medium (40-60%), and high (65-90%) RH compared at a few select temperatures. Some of these studies identified a 'U-shaped' curve of inactivation as a function of RH (*4, 5, 7*), and it has been suggested that RH affects virus inactivation by controlling evaporation of water from the aerosol particle, thus governing the concentration of inactivation-catalysing solutes (*14, 15, 16*). Beyond this, the mechanism(s) of virus inactivation in aerosol particles remain largely speculative.

A potentially powerful, yet understudied driver of airborne virus inactivation is the aerosol pH. It is established now that aerosol particles can be highly acidic (*17*), and that some enveloped viruses, including influenza virus, are sensitive to low pH (*18*). Nevertheless, the pH of expiratory aerosol particles, and hence its contribution to the inactivation of airborne viruses, remains unknown. The aerosol pH depends on the composition of the aerosol particle and the surrounding air, and it is well characterized for particulate matter equilibrated with inorganic acids and bases (*19*). Some studies have investigated the role of matrix composition on virus inactivation in particles, including its protective properties (*7, 8, 20*). However, the

impact of air composition beyond RH has been overlooked by scientists to date. To the best of our knowledge, the only attempt to inactivate airborne viruses by - likely inadvertently - modulating aerosol pH is the use of acetic acid from boiling vinegar during the 2002/03 outbreak of SARS-CoV-1 (see (*21*) and Supplementary Material).

Outdoor airborne particulate matter is often highly acidic, with pH values ranging between -1 and +5 (*17, 19*). Contrary to expectations, the strength of the acid or base contained in aerosols (expressed by its dissociation constants) may not be the dominant parameter controlling aerosol pH. Rather, the volatility of species is of importance. For example, strong organic acids like HCOOH and CH_3COOH partition negligibly to aerosol and bear a minor impact on aerosol pH for most atmospherically relevant conditions (*22*). In contrast, HNO_3 and NH_3 partition into aerosol particles and impact pH, albeit buffered by the formation of ammonium nitrate.

Indoor aerosol particles have a variety of sources, including outdoor air, human transpiration and respiration, and building materials. Indoor air tends to have lower levels of gas-phase inorganic acids (e.g., HNO_3) than outdoor air, owing to their condensation on aerosol particles as well as their efficient removal via deposition on surfaces. Human activities are a source of organic acids and NH_3 (*19, 23, 24*), often elevating their levels compared to outdoors. The ratio of indoor to outdoor concentrations is typically 0.1-0.5 for HNO_3 and 3-30 for NH_3, causing the pH of indoor aerosol particles to increase compared to outdoor levels. Operation of humidification, ventilation, and air conditioning (HVAC) systems also affect air composition (*25*) and, hence, likely the pH of indoor aerosol particles. While many outdoor and indoor aerosol particles are in equilibrium with their environment, this can only be expected for exhaled aerosol if given enough time. In the interim, freshly exhaled aerosol can change its pH considerably.

Exhaled air, before mixing into the indoor air, contains high concentrations of ammonia and is characterized by very high concentrations of CO_2 and high number densities of expiratory aerosol particles. These particles are emitted by breathing, talking, coughing or sneezing, and

contain a complex aqueous mixture of ions, proteins and surfactants. Although the pH of exhaled breath condensate has been investigated (*26*), there is no study that quantifies the pH of respiratory aerosol - especially when it equilibrates with the acidic or alkaline gases present in the indoor air within a few seconds to minutes of exhalation.

Here, we investigate the role of aerosol acidity in the inactivation of airborne influenza A virus (IAV) and two coronaviruses, SARS-CoV-2 and HCoV-229E in indoor environments. We accomplish this in three steps by first determining the pH-dependent inactivation kinetics of IAV, SARS-CoV-2 and HCoV-229E in bulk samples of representative respiratory fluids, then measuring the thermodynamic and kinetic properties of microscopic particles of these fluids, and finally jointly applying the inactivation kinetics and aerosol properties in a biophysical model to determine inactivation in the aerosol system. We then use the model to investigate the possibility of using gaseous nitric acid (HNO_3) in indoor environments at non-hazardous concentrations to lower the pH of respiratory aerosol for a wide range of sizes, and thus to effectively reduce the risk of transmission.

Kinetics of pH-mediated inactivation of influenza virus and coronavirus

Inactivation kinetics of IAV (strain A/WSN/33), SARS-CoV-2 (BetaCoV/Germany/BavPat1/2020) and HCoV-229E (strain HCoV-229E-Ren) were determined over a pH range from neutral to strongly acidic, after immersion in bulk solutions of synthetic lung fluid (SLF; see Table S1 for composition), mucus harvested from primary epithelial nasal cultures grown at air-liquid interface (nasal mucus) or aqueous citric acid/Na_2HPO_4 buffer. Figure 1 summarizes the inactivation times (here expressed as the time to reach a 99% infectivity loss) as a function of pH. All viruses were stable in all matrices at neutral pH, with inactivation times of several days. From pH 6 to 4, IAV inactivation times decreased from days to seconds, or by about five orders of magnitude. This decrease was evident in all matrices studied. It is noteworthy that inactivation in nasal mucus, which is most representative of the matrix comprising expiratory aerosol particles, is well described by SLF. However, inactivation times did depend on the

SLF concentration. Specifically, we determined IAV inactivation at three different levels of SLF enrichment (1× and 18× SLF, determined experimentally; 24× SLF, determined by extrapolation), corresponding to water activities $a_w = 0.994$, 0.8 and 0.5. This represents the fluid in equilibrium with a gas phase at 99.4%, 80% and 50% RH, i.e. from physiological equilibrium to common indoor conditions. While inactivation times in aqueous buffer, 1× SLF and nasal mucus were very similar, 18× enrichment of the SLF coincided with an increase in inactivation time by up to a factor 56 (blue triangles in Fig. 1). This protective effect of concentrated SLF was most prominent around the optimal pH for A/WSN/33 viral fusion of $\sim$ 5.1 (*27*). Coronaviruses were less affected by acidic pH than IAV. Both, SARS-CoV-2 and HCoV-229E remained largely stable down to pH 3, where their inactivation still required 24 hours. When further decreasing pH down to 2, the inactivation times rapidly reduced to < 10 seconds for SARS-CoV-2, but never dropped below 2 hours for HCoV-229E. Compared to aqueous buffer, SLF provided some protection against inactivation below pH 3, both at 1× and 5× SLF concentrations (while measurements for pH < 3 in 18× SLF were not possible due to precipitation). The measured differences in pH-sensitivities between IAV and the coronaviruses may be explained by their different mechanisms of virus entry into host cells. IAV relies on an acid-induced conformational change in haemagglutinin during endosomal entry. This conformational change is irreversible (*28*); if IAV encounters the fusion pH (typically pH < 5.5) outside the host cell, e.g. whilst within an aerosol particle, the acid-triggered haemagglutinin can no longer bind to host-cell receptors and the virus is inactivated. Conversely, the spike glycoprotein of coronaviruses becomes fusion competent through cleavage by host proteases, instead of relying on acidic pH triggering conformational changes (*29*). The different behavior of SARS-CoV-2 and HCoV-229E at pH < 3 remains unclear.

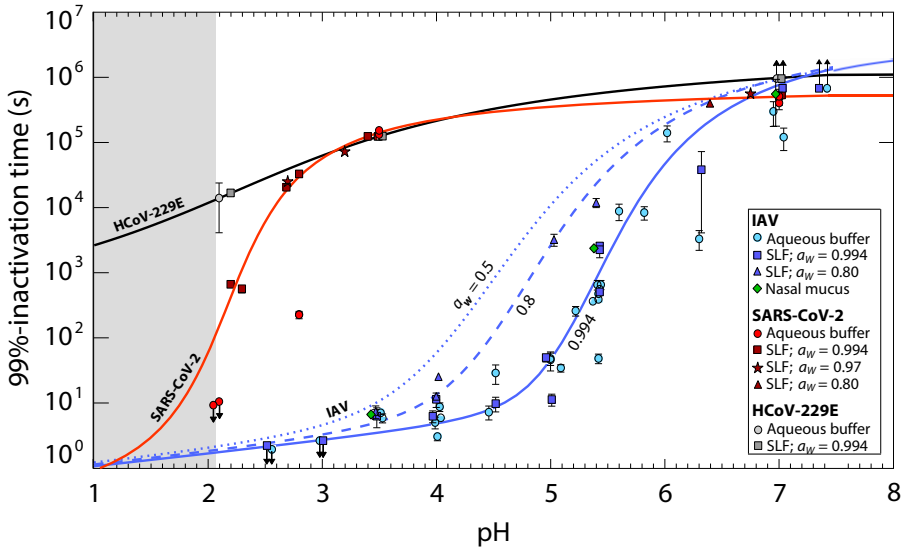

Figure 1. Time required for 99% titer reduction of influenza A virus (IAV), SARS-CoV-2 and human coronavirus HCoV-229E measured in various bulk media ($>$ 10 µl) at 22°C. Data points represent inactivation times in aqueous citric acid/Na_2HPO_4 buffer, synthetic lung fluid (SLF) or nasal mucus with pH between 7.4 and 2. SLF concentrations correspond to water activity $a_w = 0.994$ (1$\times$ SLF; squares), $a_w = 0.97$ (5$\times$ SLF; stars) and $a_w = 0.8$ (18$\times$ SLF; triangles); buffer (circles) and nasal mucus (diamonds) correspond to $a_w \sim 0.99$. Each experimental condition was tested in replicate with error bars indicating 95% confidence intervals. While IAV displays a pronounced reduction in infectivity around pH 5, SARS-CoV-2 develops a similar reduction only close to pH 2, and HCoV-229E is largely pH-insensitive. Solid lines are arctan fits to SLF data with $a_w = 0.994$ (blue: IAV; red: SARS-CoV-2; black: HCoV-229E). The dashed line is an arctan fit to the SLF data with $a_w = 0.80$. The dotted line is an extrapolation to $a_w = 0.5$ (24$\times$ SLF). Upward arrows indicate insignificant change in titer over the course of the experiment, and downward arrows indicate inactivation below the level of detection at all measured times. The fitted curves below pH 2 (grey shaded aera) are extrapolated with high uncertainty. Examples of measured inactivation curves are shown in Fig. S1. The arctan fit equations, which are also used for the model simulations, are given by Eqns. S28, S29, and S30.

Thermodynamics and diffusion kinetics of expiratory particles

While Figure 1 shows the pH that must be attained in the aerosol particles for rapid virus inactivation, it lacks information on aerosol particle pH after exhalation into indoor air. To model the pH in these particles it is essential to know the particle composition in thermodynamic equilibrium (liquid water content), as well as the kinetics that determine how rapidly the equilibrium is approached (water and ion diffusion coefficients). To obtain this information, we measured thermodynamic (equilibrium) and kinetic (diffusion-controlled) properties

of individual micrometer-sized SLF and nasal mucus particles levitated contact-free in an electrodynamic balance (EDB). Each particle was exposed to prescribed changes in RH (see Fig. 2).

Figure 2A shows two moistening/drying cycles of an SLF particle obtained over a period of two days. They allow determination of the particle equilibrium composition (water content or mass fraction of solutes, see Fig. S2A) during time intervals with slowly changing RH. The particle clearly takes up and loses water when the RH is changed. It has a size growth factor at 90% RH of 1.3 (see also Fig. S3) and deliquesces at 75%, indicating that NaCl is the predominant salt in the particle. Nasal mucus shows a similar size growth, but deliquesces over an RH range of 55 to 70%, indicating that it contains significant amounts of other salts (Fig. S3). We have no evidence for liquid-liquid phase separation in any of these particles (Fig. S4A and S5) but Mie-Resonance spectra indicate inhomogenities in the particles even at high RH.

The kinetics of water uptake/loss as derived from periods with rapid RH change or efflorescence are highlighted in Fig. 2. Figure 2B zooms in on one efflorescence event, first showing rapid water loss (< 10 s), then switching to a much slower rate of water loss over the next hour. This two-stage diffusion process was confirmed in measurements of additional SLF and nasal mucus particles (see Fig. S6). We attribute the fast process to an initial dendritic growth of an NaCl crystal (Fig. S4A-C), which ends abruptly when the crystal reaches the droplet surface, followed by a slow crystal growth mode (Fig. S4D). Initially, crystal growth is limited by the liquid phase diffusivity of water molecules with $D_{\ell,\mathrm{H_2O}} > 10^{-7}$ cm^2/s (Fig. 2C), which is expelled from the particle as long as water activity is still high. Subsequently, the slow crystal growth is limited by the diffusivities of Na^+ and Cl^- ions through the progressively viscous liquid to the crystal (Fig. S4D). From Figs. 2B and S4D we estimate the ion diffusion coefficient to be about $D^*_{\ell,\mathrm{ions}} \approx 10^{-10}$ cm^2/s, which determines the low rate of continued loss of water molecules. The diffusion coefficients determined in this way are "effective" (indicated by a star), as they represent the molecular diffusivities under the specific morphological

conditions associated with the dendritic growth of the salt crystals inside the droplets (see next section for details on how these diffusion coefficients were further constrained).

In summary, independent of the exact thermodynamic equilibrium state of the particles, our results demonstrate that SLF as well as nasal mucus show a clear diffusion limitation for ions. In contrast, water diffusion in SLF and nasal mucus remains fast even when RH is low. This continuous, rapid diffusion of water indicates that SLF and nasal mucus do not form diffusion-inhibiting, semisolid phase states such as those recently reported by others in particlets containing model respiratory compounds (*30*).

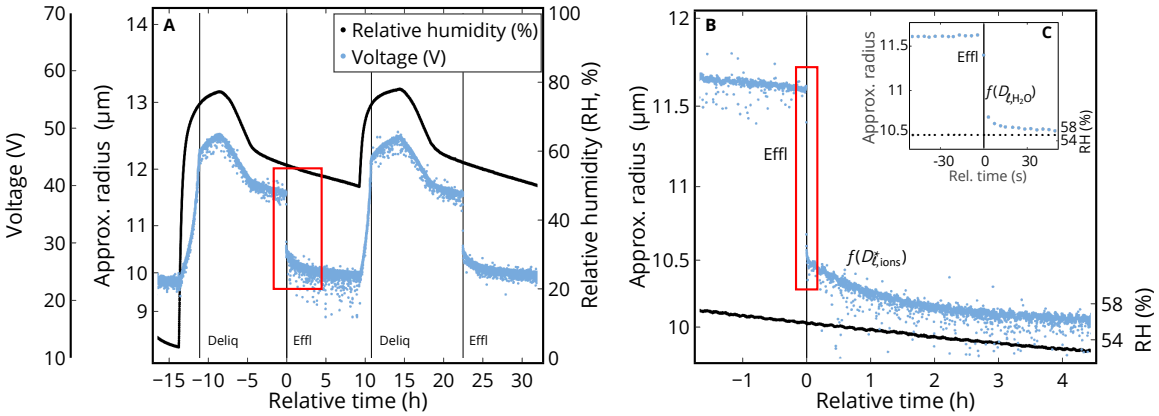

Figure 2. Measured hygroscopicity cycles of a synthetic lung fluid (SLF) particle in an electrodynamic balance (EDB) forced by prescribed changes in relative humidity (RH). The voltage required to balance the particle in the EDB against gravitational settling and aerodynamic forces is a measure of the particle's mass-to-charge ratio, allowing the particle radius R to be estimated. (**A**) Two humidification cycles of an SLF particle with a dry radius $R_0 \sim 9.7$ µm. The experiment spanned about 2 days with slow humidity changes, allowing the thermodynamic and kinetic properties of SLF to be determined. Deliquescence/efflorescence points are marked by "Deliq/Effl". (**B**) Zoom on the drying phase (red box in (A)) with salts in the droplet (mainly NaCl) efflorescing around 56% RH (black line): very fast initial crystal growth (< 10 s) with rapid loss of H_2O from the particle, followed by slow further crystal growth (1 h). The latter is caused by the abrupt switch from H_2O diffusion to the diffusion of Na^+ and Cl^- ions through the viscous liquid, resulting in an ion diffusion coefficient of $D^*_{\ell,\mathrm{ions}} \approx 10^{-10}$ cm^2/s. The insert (**C**) highlights the minute before and after efflorescence, which allows a lower bound of the H_2O diffusivity (namely $D_{\ell,\mathrm{H_2O}} > 10^{-7}$ cm^2/s) to be determined.

Biophysical model of inactivation in expiratory aerosol particles

Only the combination of the virological bulk phase data (Fig. 1) with the microphysical aerosol thermodynamics (vapor pressures and activity coefficients) and kinetics (Figs. 2 and S7) allows the pH attained in the aerosol particles and the resulting rates of viral inactivation, to be determined. Thus, the virological and microphysical data were combined as input for a multi-layer Respiratory Aerosol Model (ResAM). ResAM is a biophysical model that simulates the composition and pH changes inside an expiratory particle during exhalation, and determines the impact of these changes on virus infectivity (see section "Biophysical modeling" in the Supplementary Material). The model performs calculations for particles of selectable size (from 20 nm to 1 mm) with a liquid phase composed of organic and inorganic species representative of human respiratory fluids S1 (more detail in the Supplementary Material). It takes account of diffusion in the gaseous and condensed phase, vapor pressures, heat transfer, deliquescence, efflorescence, species dissociation, and activity coefficients due to electrolytic ion interactions (see Tables S2, S3). Ultimately, ResAM computes the species distribution and their activity in the liquid, the resulting pH, and the corresponding virus inactivation rates as function of time and of the radial coordinate within the particle.

When RH changes are slow, the measured mass fraction of solutes in SLF as a function of RH allows the model thermodynamics to be constrained (Fig. S2B). Under thermodynamic equilibrium conditions the model captures the mass fraction of solutes along the deliquesced and effloresced branches of the particle reasonably well. However, only after kinetic effects (ion and water diffusivities) are also taken into account does the model accurately reproduce the solute composition curve along the deliquesced branch. This demonstrates that even when RH changes are slow (raising RH from 50% to 70% in over one hour), kinetics cannot be neglected.

For rapidly evaporating expiratory particles, kinetics effects are even more critical. By matching the model to the fast changes during the efflorescence and deliquescence processes, ion diffusion coefficients can be derived for different water activities. Interpolation together

with literature data in dilute conditions yields $D_{\ell,\mathrm{H_2O}}$, $D_{\ell,\mathrm{Na^+}}$, and $D_{\ell,\mathrm{Cl^-}}$ (for details see Fig. S7D). Other neutral species, cations and anions are treated accordingly, scaled with their infinite dilution values (see Supplementary Material).

As an example, Fig. 3 shows the evolution of the physicochemical conditions within an expiratory particle with 1 μm initial radius during transition from nasal to typical indoor air conditions with 50% RH (Table S1), and the concomitant inactivation of IAV and SARS-CoV-2 contained within the particle. The rapid loss of water leads to concentration of the organics and salts, to the point when NaCl effloresces. Nitric acid from the indoor air enters the particle readily, lowering its pH from an initial value of 6.6 (resulting from the high concentrations of CO_2 and NH_3 in the exhaled air) to pH 5 within ~ 10 s. This, in turn, pulls NH_3 into the particle, partly compensating the acidification. The pH further decreases to ~ 4 within 2 minutes, then slowly approaches pH 3.7 due to further uptake of HNO_3 from the room air. This result confirms the importance of trace gases in determining the pH of indoor aerosol particles (*24*). If only CO_2 is considered, its volatilization from the particle would lead to an expected increase in pH after exhalation (*31*). Owing to aerosol acidification, rapid influenza virus inactivation occurs at ~ 2 minutes, whereas SARS-CoV-2 (and the even more pH-tolerant HCoV-229E) remain infectious.

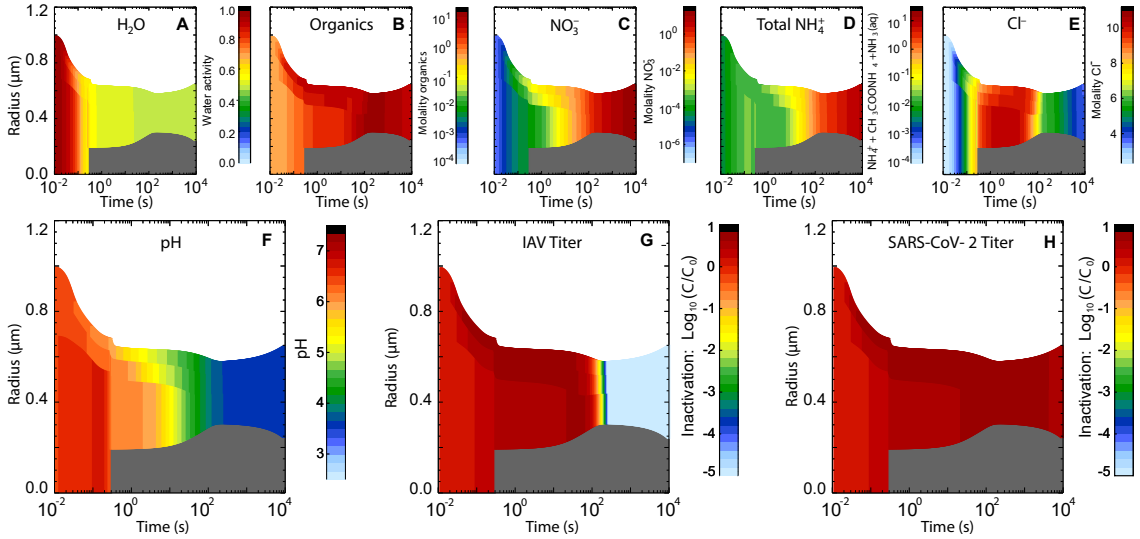

Figure 3. Evolution of physicochemical conditions within a respiratory particle leading to inactivation of trapped viruses during the transition from nasal to typical indoor air conditions, modeled with ResAM. The initial radius of the particle is 1 μm. Thermodynamic and kinetic properties are those of synthetic lung fluid (SLF, see Fig. 2 and Table S1). The indoor air conditions are set at 20°C and 50% RH (see Fig. S8 for the corresponding depiction of physicochemical conditions at 80% RH). The exhaled air is assumed to mix into the indoor air using a turbulent eddy diffusion coefficient of 50 cm^2/s (*32*). The temporal evolution of gas phase mixing ratios is shown in Fig. S20. The gas phase compositions of exhaled and typical indoor air are given in Table S4. Within 0.3 s, the particle shrinks to 0.7 μm due to rapid H_2O loss, causing NaCl to effloresce (grey core). The particle then reaches 0.6 μm within 2 minutes due to further crystal growth, after which it slowly grows again due to coupled HNO_3 and NH_3 uptake and HCl loss. ResAM models the physicochemical changes in particles including (**A**) water activity, (**B**) molality of organics, (**C**) NO_3^- (resulting from the deprotonation of HNO_3), (**D**) molality of total ammonium, (**E**) molality of Cl^-, (**F**) pH, as well as inactivation of (**G**) IAV and (**H**) SARS-CoV-2 (decadal logarithm of virus titer C at time t relative to initial virus titer C_0).

Inactivation times vary with particle size: larger droplets take longer to reach low pH than smaller ones as they are impeded by longer diffusion paths of the relevant molecules (mainly HNO_3 and NH_3) or ions through both the air and liquid phases. The black line in Fig. 4C illustrates this relationship for IAV, showing 99% inactivation after about 2 minutes in particles with radii < 1 μm, but longer than 5 days for millimeter-sized particles. As a rule of thumb, a 10-fold increase in particle size leads to roughly a 10-fold increase in IAV inactivation time under typical indoor conditions. Conversely, the black line in Fig. 4D for SARS-CoV-2 shows

that inactivation is inefficient for SARS-CoV-2, irrespective of particle size.

Inactivation times for both IAV and SARS-CoV-2 can be greatly reduced if the indoor air is slightly acidified, provided that the gaseous acid molecules meet two conditions: their volatility must be sufficiently low, such that they readily partition from the gas phase to the condensed phase, and, once dissolved, they must be sufficiently strong acids to overcome any pH buffering by the particle matrix. Figure 4 compares the aerosol pH in typical indoor air (panel A) with that in air enriched with 50 ppb HNO_3 (panel B). This concentration of HNO_3 is well below legal 8-h exposure thresholds (0.5 ppm (*33*) or 2 ppm (*34*)). Notably, 50 ppb HNO_3 reduces the time to reach an aerosol pH of 4 from minutes to seconds. More importantly, 50 ppb also allowed the pH value to drop below 2, which is required for efficient SARS-CoV-2 inactivation (Fig. 1). For comparison, enriching the air with the more volatile and weaker acetic acid at concentrations below exposure threshold values could not achieve this, see Fig. S9. The dark blue lines in Fig. 4C-D show the resulting inactivation times for IAV and SARS-CoV-2 (and Fig. S10 for HCoV-229E) as a function of particle radius. Remarkably, inactivation times of SARS-CoV-2 diminished by 4-5 orders of magnitude compared to typical indoor air (black lines). For particles with radii < 1 μm, which constitutes the majority of expiratory particles (see panel E), inactivation is expected to occur within 30 s.

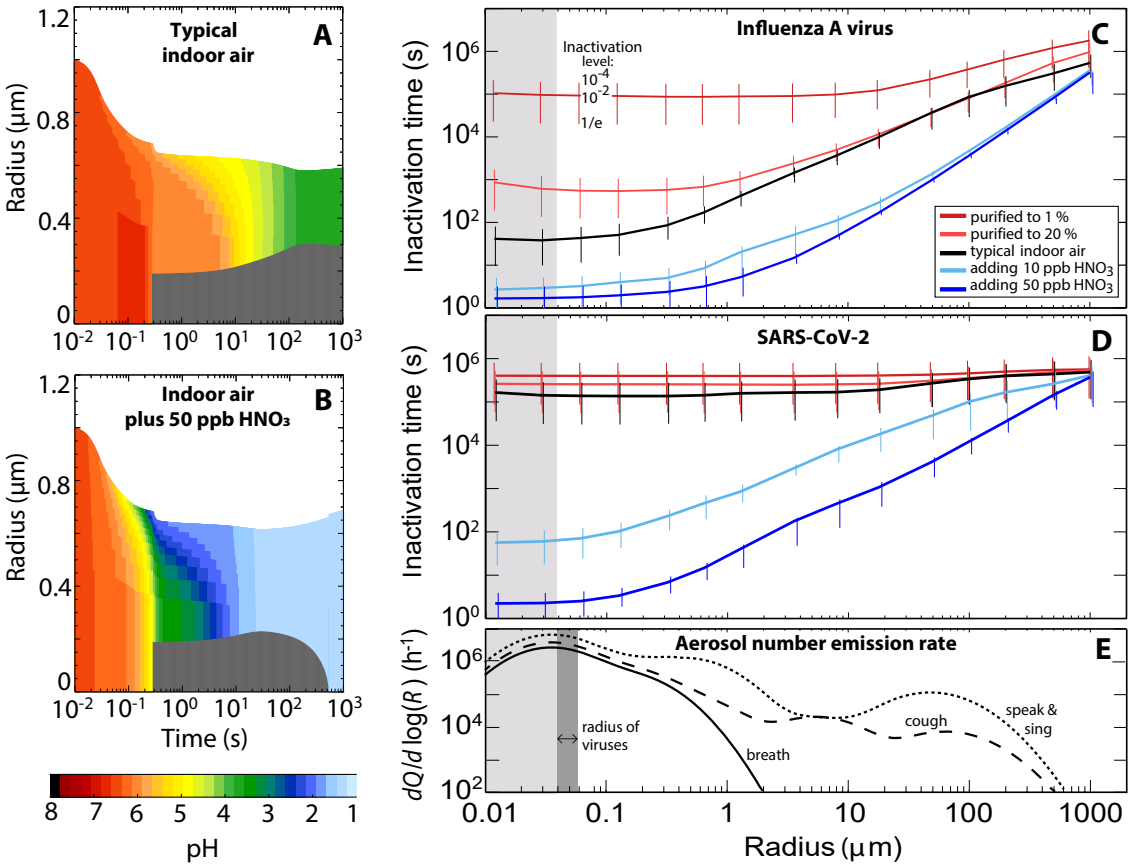

Figure 4. Impact of nitric acid vapor (HNO_3) in indoor air on virus inactivation in expiratory particles. (**A**) Modeled pH value in an expiratory particle with properties of synthetic lung fluid with initially 1 µm radius in indoor air (20°C, 50% RH) of typical composition (identical to 3F, but with different color scale). (**B**) Same, but in indoor air enriched with 50 ppb HNO_3, reducing the time to reach pH 4 from 2 minutes to less than 2 seconds. (**C and D**) Inactivation times of IAV and SARS-CoV-2 as function of particle radius under various conditions: indoor air with typical composition (black), enriched with 10 or 50 ppb HNO_3 (blue), or purified air with HNO_3 and NH_3 reduced to 20% or 1% (red). Whiskers show reductions of virus load to 10^{-4} (upper end), 10^{-2} (intersection with line) and 1/e (lower end). The exhaled air mixes with the indoor air by turbulent eddy diffusion (see Fig. 3). For sensitivity tests see Figs. S11B and S12B. The gas phase compositions of exhaled air and the various cases of indoor air are defined in Table S4. (**E**) Mean size distribution (*35*) of number emission rates of expiratory aerosol particles ($dQ/d\log(R)$) for breathing (solid line), speaking and singing (dotted line) and coughing (dashed line). Dark grey range indicates virus radii. Light grey shading shows conditions for particles smaller than a virus, referring to an equivalent coating volume with inactivation times indicated. (Radius values in (C)-(E) refer to the particle size 1 s after exhalation.)

While an enrichment of acidic gases in air leads to an acceleration of IAV and SARS-CoV-2

inactivation, the depletion of these gases, for instance by air filtration, has the opposite effect. It is well-known that concentrations of strong inorganic acids, such as HNO_3, are lower indoors than outdoors by at least a factor 2, and in buildings with special air purification, such as museums and libraries, by factors 10-80 (*24*). If air is purified to contain only a fraction of the initial trace gas concentrations (see Table S4), the aerosol pH increases compared to typical indoor air and intermittently reaches neutral or even slightly alkaline values (up to pH 8.4 in particles with 5 μm radius in air purified to 1%). As a result, air purification is expected to enhance virus persistence, especially for IAV, as indicated by the red curves in Fig. 4.

To validate the model results, we compared published inactivation data for aerosolized IAV and SARS-CoV-2 obtained in rotating drum experiments with inactivation times estimated by ResAM (Figures S13 and S14 and supplementary text). For both viruses, modelled and measured inactivation times exhibited similar trends as a function of RH. For IAV, measured inactivation times are consistent with ResAM predictions for experiments conducted in partly purified air, as is expected for rotating drum experiments. The comparison with SARS-CoV-2 is inconclusive, because of the wide scatter in the experimental data. However, ResAM predictions fall within the range of measured inactivation times. Given the importance of semi-volatile acids and bases for inactivation, further model validation should include inactivation times measured in aerosol experiments under well-known air compositions, including the presence of HNO_3.

Management of airborne transmission risks

Given the high pH sensitivity of many viruses (*18, 36, 37, 38*) and the readiness of expiratory aerosol particles for acidification, we next investigated the extent to which the modification of indoor air composition could mitigate the risk of virus transmission. To this end, we consider a ventilated room with occupants who exhale aerosol containing infectious viruses. We further make the assumption that, given the low concentration of airborne viruses, the transmission risk is directly proportional to the infectious virus concentration, respectively inhalation dose. We use the term "relative risk of transmission" to express how the risk changes from standard

conditions (here typical indoor air according to Table S4) compared to air slightly enriched by HNO_3 or air that has been purified.

For the ventilated room we assume steady-state conditions where the exhalation defines the source of virus, which is balanced by three sinks, namely air exchange through ventilation, aerosol deposition, and pH-moderated virus inactivation within the aerosol particles (see Supplementary Material). We describe the virus source by the mean size distributions of number emission rates of expiratory aerosol particles (Fig. 4E) and assume each particle with radius > 50 nm to carry one virus irrespective of size. We describe the virus sinks by expressing ventilation by Air Change per Hour (ACH, mixing ventilation), applying mean aerosol deposition rates (*39*), and computing the inactivation rates similar to Fig. 4C,D. This allows the airborne viral load and, thus, the relative risk of transmission, to be calculated as displayed in Fig. 5 for IAV and SARS-CoV-2 (and Fig. S15 for HCoV-229E). Black bars show the results for typical indoor conditions, blue bars indicate an enrichment of HNO_3 to 10 or 50 ppb, and red bars indicate purification of air to 20% or 1% of trace gases (see Table S4).

The results are unambiguous: while adding 50 ppb HNO_3 only has a moderate impact on HCoV-229E (Figs. S10 and S15), it promises to diminish the relative risk of transmission of IAV by a factor of ~ 20 and of SARS-CoV-2 by a factor of 800 in rooms with ACH 2. Using HNO_3 is a more effective measure than increasing ventilation from ACH2 to ACH10, which for SARS-CoV-2 leads to a mere dilution by a factor 5 and for IAV does not help at all as the IAV 99%-inactivation time in typical indoor air is already short (2 minutes).

The ResAM estimates for purified air with significant reduction of trace gases (red bars) are also striking. While even normal air conditioning systems with air filters can lead to a reduction in "sticky" molecules such as HNO_3 (*40*), acid removal is likely even more pronounced in museums, libraries or hospitals with activated carbon filters (*24*). In such public buildings, the relative risk of IAV transmission can increase significantly compared to buildings supplied with unfiltered outside air.

Here we demonstrate that a significant reduction in transmission risk can be achieved by

air enrichment with HNO_3 levels that correspond to less than 10% of the legal exposure thresholds (*33, 34*). We therefore expect that the resulting acid exposure will not cause harmful effects on human health. Nevertheless, future studies should investigate the effects of acid accumulation in indoor air on the microbiome and immune response in the respiratory tract. In addition, ResAM should be further refined to include a greater diversity of respiratory matrices. Aerosol particles emitted during different human activities (e.g., coughing, singing) differ in their production mechanisms and site of origin in the respiratory tract, and hence in their matrix composition. The two matrices considered in this work - SLF and nasal mucus - have comparable thermodynamic and kinetic properties as well as a similar pH-dependence of viral inactivation. However, we cannot exclude that additional respiratory matrices found in expiratory aerosol plumes (e.g., saliva) exhibit divergent properties (*30, 41*). Despite these current unknowns, targeted regulation of aerosol pH promises profound positive effects on virus transmission and disease mitigation strategies.

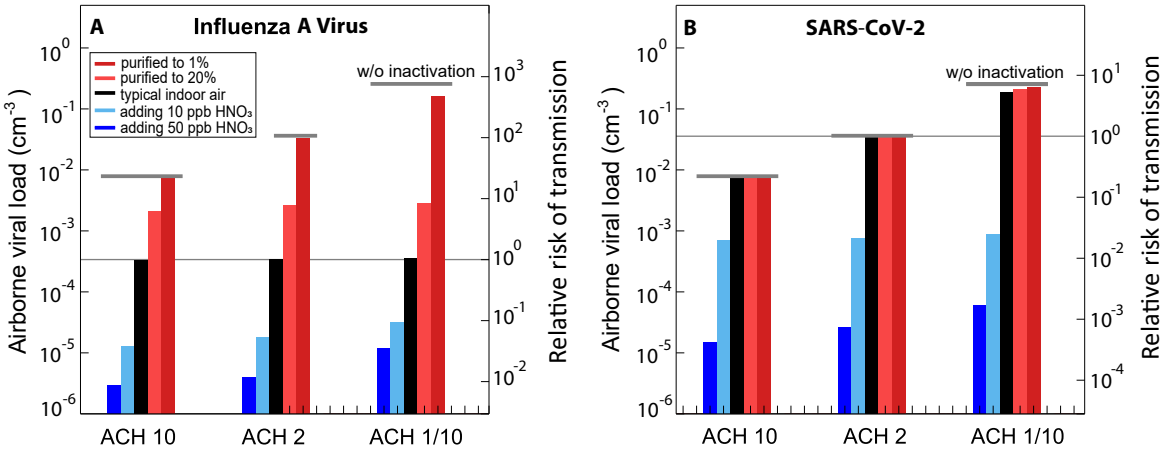

Figure 5. Airborne viral load (# viruses per volume of air) and relative risk of transmission of (A) IAV and (B) SARS-CoV-2 infection in a room subject to various air treatments, such as addition of HNO_3 or supply of purified air with different ventilation rates, Air Changes per Hour (ACH). The room is assumed to accommodate one infected person per 10 m^3 of air volume, emitting virus-laden aerosol by normal breathing (solid curve in Figure 4E), and assuming one infectious virus per aerosol particle. (Corresponding plots assuming a virus concentration that is proportional to the size of the aerosol particles are shown in Fig. S16.) Steady state virus loading, i.e. number of infectious viruses per cubic centimeter of air (left axes), is calculated as the balance of exhaled viruses and their removal by ventilation, deposition, and inactivation. Results are shown for three different ventilation strengths. Virus inactivation is calculated according to Figure 4C-D, starting from radius 0.05 μm. Note, that the mixing speed of the exhalation plume with indoor air depends on ACH (following (*32*), see Supplementary Text). Right axes show the transmission risk under these treatments relative to the risk in a room with typical indoor air (see Table S4) and ACH 2 (thin horizontal line). Typical indoor air is shown by black bars, filtered air with removal of trace gases to 20% and 1% by red bars, and air enriched with 10 or 50 ppb HNO_3 by blue bars. Thick grey horizontal lines indicate the viral load and relative transmission risk in the absence of any inactivation. Results for 2 and 5 ppb HNO_3 are shown in Fig. S17. Results for HCoV-229E, along with analogous analyses for coughing and speaking/singing are shown in Fig. S15.

References

1. Paget, J. *et al.* Global mortality associated with seasonal influenza epidemics: New burden estimates and predictors from the GLaMOR Project. *Journal of Global Health* **9**, DOI: 10.7189/JOGH.09.020421 (2019).

2. Clarification of terminology: In physical chemistry, an "aerosol" is a system of colloidal particles dispersed in a fluid, such as air. An "aerosol particle" refers to one single condensed-phase element in such an ensemble, which may be solid, liquid or mixed phase. Correspondingly, a "droplet" refers to any liquid aerosol particle, regardless of particle size. In contrast, in epidemiological or virological parlance "aerosol" or "aerosol particle" usually means a very small ($d \lesssim 1\mu$m) airborne particle, whereas "droplet" is used as its larger counterpart ($d \gg 1\mu$m). To avoid this confusion, we use the term "particle" to refer to any liquid or mixed-phase respiratory particle of whatever size. Furthermore, we avoid the virological term "virus particle" and use "virus" instead.

3. Wang, C. C. *et al.* Airborne transmission of respiratory viruses. *Science* **373**, eabd9149, DOI: 10.1126/science.abd9149 (2021).

4. Shechmeister, I. L. Studies on the experimental epidemiology of respiratory infections. III. Certain aspects of the behavior of type A influenza virus as an air-borne cloud. *The Journal of Infectious Diseases* **87**, 128–132, DOI: 10.1093/INFDIS/87.2.128 (1950).

5. Hemmes, J. H., Winkler, K. C. & Kool, S. M. Virus survival as a seasonal factor in influenza and poliomyelitis. *Nature* **188**, 430–431, DOI: 10.1038/188430a0 (1960).

6. Harper, G. J. Airborne micro-organisms: survival tests with four viruses. *The Journal of hygiene* **59**, 479–486, DOI: 10.1017/s0022172400039176 (1961).

7. Schaffer, F. L., Soergel, M. E. & Straube, D. C. Survival of airborne influenza virus: Effects of propagating host, relative humidity, and composition of spray fluids. *Archives of Virology* **51**, 263–273, DOI: 10.1007/BF01317930 (1976).

8. Kormuth, K. A. *et al.* Influenza virus infectivity is retained in aerosols and droplets independent of relative humidity. *The Journal of Infectious Diseases* **218**, 739–747, DOI: 10.1093/infdis/jiy221 (2018).

9. Schuit, M. *et al.* The influence of simulated sunlight on the inactivation of influenza virus in aerosols. *The Journal of infectious diseases* **221**, 372—378, DOI: 10.1093/infdis/jiz582 (2020).

10. Schuit, M. *et al.* Airborne SARS-CoV-2 Is Rapidly Inactivated by Simulated Sunlight. *The Journal of Infectious Diseases* **222**, 564–571, DOI: 10.1093/infdis/jiaa334 (2020).

11. Dabisch, P. *et al.* The influence of temperature, humidity, and simulated sunlight on the infectivity of SARS-CoV-2 in aerosols. *Aerosol Science and Technology* **55**, 142–153, DOI: 10.1080/02786826.2020.1829536 (2021).

12. van Doremalen, N. *et al.* Aerosol and surface stability of SARS-CoV-2 as compared with SARS-CoV-1. *New England Journal of Medicine* **382**, 1564–1567, DOI: 10.1056/NEJMc2004973 (2020).

13. Ijaz, M. K., Brunner, A. H., Sattar, S. A., Nair, R. C. & Johnson-Lussenburg, C. M. Survival characteristics of airborne human coronavirus 229E. *Journal of General Virology* **66**, 2743–2748, DOI: 10.1099/0022-1317-66-12-2743 (1985).

14. Marr, L. C., Tang, J. W., Van Mullekom, J. & Lakdawala, S. S. Mechanistic insights into the effect of humidity on airborne influenza virus survival, transmission and incidence. *Journal of The Royal Society Interface* **16**, 20180298, DOI: 10.1098/rsif.2018.0298 (2019).

15. Lin, K. & Marr, L. C. Humidity-dependent decay of viruses, but not bacteria, in aerosols and droplets follows disinfection kinetics. *Environmental Science & Technology* **54**, 1024–1032, DOI: 10.1021/acs.est.9b04959 (2020).

16. Morris, D. H. *et al.* Mechanistic theory predicts the effects of temperature and humidity

on inactivation of SARS-CoV-2 and other enveloped viruses. *eLife* **10**, DOI: 10.7554/ELIFE.65902 (2021).

17. Weber, R. J., Guo, H., Russell, A. G. & Nenes, A. High aerosol acidity despite declining atmospheric sulfate concentrations over the past 15 years. *Nature Geoscience 2016 9:4* **9**, 282–285, DOI: 10.1038/ngeo2665 (2016).

18. Scholtissek, C. Stability of infectious influenza A viruses to treatment at low pH and heating. *Archives of Virology* **85**, 1–11, DOI: 10.1007/BF01317001 (1985).

19. Pye, H. O. *et al.* The acidity of atmospheric particles and clouds. *Atmospheric Chemistry and Physics* **20**, 4809–4888, DOI: 10.5194/ACP-20-4809-2020 (2020).

20. Yang, W., Elankumaran, S. & Marr, L. C. Relationship between Humidity and Influenza A Viability in Droplets and Implications for Influenza's Seasonality. *PLoS ONE* **7**, e46789, DOI: 10.1371/journal.pone.0046789 (2012).

21. Huang, Y. The SARS epidemic and its aftermath in China: a political perspective. In *Learning from SARS - Preparing for the Next Disease Outbreak: Workshop Summary*, 116 – 136 (Institute of Medicine, The National Academies Press, Washington DC, 2004).

22. Nah, T. *et al.* Characterization of aerosol composition, aerosol acidity, and organic acid partitioning at an agriculturally intensive rural southeastern US site. *Atmospheric Chemistry and Physics* **18**, 11471–11491, DOI: 10.5194/ACP-18-11471-2018 (2018).

23. Brauer, M., Koutrakis, P., Keeler, G. J. & Spengler, J. D. Indoor and outdoor concentrations of inorganic acidic aerosols and gases. *Journal of the Air and Waste Management Association* **41**, 171–181, DOI: 10.1080/10473289.1991.10466834 (1991).

24. Nazaroff, W. W. & Weschler, C. J. Indoor acids and bases. *Indoor Air* **30**, 559–644, DOI: 10.1111/ina.12670 (2020).

25. Ampollini, L. *et al.* Observations and contributions of real-time indoor ammonia concentrations during HOMEChem. *Environmental Science and Technology* **53**, 8591–8598,

DOI: 10.1021/acs.est.9b02157 (2019).

26. Vaughan, J. *et al.* Exhaled breath condensate pH is a robust and reproducible assay of airway acidity. *European Respiratory Journal* **22**, 889–894, DOI: 10.1183/09031936.03.00038803 (2003).

27. Galloway, S. E., Reed, M. L., Russell, C. J. & Steinhauer, D. A. Influenza HA subtypes demonstrate divergent phenotypes for cleavage activation and pH of fusion: implications for host range and adaptation. *PLoS pathogens* **9**, e1003151–e1003151, DOI: 10.1371/journal.ppat.1003151 (2013).

28. Bullough, P. A., Hughson, F. M., Skehel, J. J. & Wiley, D. C. Structure of influenza haemagglutinin at the pH of membrane fusion. *Nature* **371**, 37–43, DOI: 10.1038/371037a0 (1994).

29. Jackson, C. B., Farzan, M., Chen, B. & Choe, H. Mechanisms of SARS-CoV-2 entry into cells. *Nature reviews. Molecular cell biology* **23**, 3–20, DOI: 10.1038/s41580-021-00418-x (2022).

30. Huynh, E. *et al.* Evidence for a semisolid phase state of aerosols and droplets relevant to the airborne and surface survival of pathogens. *Proceedings of the National Academy of Sciences* **119**, e2109750119, DOI: 10.1073/PNAS.2109750119/VIDEO-1 (2022).

31. Oswin, H. P. *et al.* Measuring stability of virus in aerosols under varying environmental conditions. *Aerosol Science and Technology* **55**, 1315–1320, DOI: 10.1080/02786826.2021.1976718 (2021).

32. Shao, Y., Ramachandran, S., Arnold, S. & Ramachandran, G. Turbulent eddy diffusion models in exposure assessment - Determination of the eddy diffusion coefficient. *Journal of Occupational and Environmental Hygiene* **14**, 195–206, DOI: 10.1080/15459624.2016.1238476 (2017).

33. The National Institute for Occupational Safety and Health (NIOSH) - Center of Disease

Control and Prevention (CDC). https://www.cdc.gov/niosh/npg/npgd0447.html: Time-weighted average (TWA) of the Permissible Exposure Limit (PEL), legal 8-hour limit in the United States for exposure of an employee 2 ppm for HNO_3 (2019).

34. German Social Accident Insurance (DGUV). https://limitvalue.ifa.dguv.de/: National Occupational Exposure Limits (OELs) in the European Union, legal 8-hour limit, 0.5 - 2 ppm for HNO_3, depending on country (2022).

35. Pöhlker, M. L. *et al.* https://arxiv.org/abs/2103.01188: Respiratory aerosols and droplets in the transmission of infectious diseases. *arXiv* **preprint**, DOI: 10.48550/arXiv.2103.01188 (2021).

36. Nicola, A. V., McEvoy, A. M. & Straus, S. E. Roles for endocytosis and low pH in herpes simplex virus entry into HeLa and chinese hamster ovary cells. *Journal of Virology* **77**, 5324–5332, DOI: 10.1128/jvi.77.9.5324-5332.2003 (2003).

37. Ausar, S. F. *et al.* Analysis of the thermal and pH stability of human respiratory syncytial virus. *Molecular Pharmaceutics* **2**, 491–499, DOI: 10.1021/mp0500465 (2005).

38. Darnell, M. E., Subbarao, K., Feinstone, S. M. & Taylor, D. R. Inactivation of the coronavirus that induces severe acute respiratory syndrome, SARS-CoV. *Journal of virological methods* **121**, 85–91, DOI: 10.1016/J.JVIROMET.2004.06.006 (2004).

39. Fogh, C. L., Byrne, M. A., Roed, J. & Goddard, A. J. Size specific indoor aerosol deposition measurements and derived I/O concentrations ratios. *Atmospheric Environment* **31**, 2193–2203, DOI: 10.1016/S1352-2310(97)00037-X (1997).

40. Neuman, J. A., Huey, L. G., Ryerson, T. B. & Fahey, D. W. Study of inlet materials for sampling atmospheric nitric acid. *Environmental Science and Technology* **33**, 1133–1136, DOI: 10.1021/es980767f (1999).

41. Groth, R., Cravigan, L. T., Niazi, S., Ristovski, Z. & Johnson, G. R. In situ measurements of human cough aerosol hygroscopicity. *Journal of the Royal Society Interface* **18**, DOI:

10.1098/rsif.2021.0209 (2021).

42. van den Worm, S. H. E. *et al.* Reverse genetics of SARS-related coronavirus using vaccinia virus-based recombination. *PLoS ONE* **7**, e32857, DOI: 10.1371/journal.pone.0032857 (2012).

43. Wölfel, R. *et al.* Virological assessment of hospitalized patients with COVID-2019. *Nature* **581**, 465–469, DOI: 10.1038/s41586-020-2196-x (2020).

44. Spieler, E. E., Moritz, E., Stertz, S. & Hale, B. G. Application of a biologically contained reporter system to study gain-of-function H5N1 influenza A viruses with pandemic potential. *mSphere* **5**, 00423–20, DOI: 10.1128/mSphere.00423-20 (2020).

45. Bicer, E. M. *Compositional characterisation of human respiratory tract lining fluids for the design of disease specific simulants*. Ph.D. thesis, King's College London (2014).

46. Hassoun, M., Royall, P. G., Parry, M., Harvey, R. D. & Forbes, B. Design and development of a biorelevant simulated human lung fluid. *Journal of Drug Delivery Science and Technology* **47**, 485–491, DOI: 10.1016/j.jddst.2018.08.006 (2018).

47. Busnadiego, I. *et al.* Antiviral activity of type I, II, and III interferons counterbalances ACE2 inducibility and restricts SARS-CoV-2. *mBio* **11**, 01928–20, DOI: 10.1128/mBio.01928-20 (2020).

48. Davis, E. J., Buehler, M. F. & Ward, T. L. The double-ring electrodynamic balance for microparticle characterization. *Review of Scientific Instruments* **61**, 1281–1288, DOI: 10.1063/1.1141227 (1990).

49. Colberg, C. A., Krieger, U. K. & Peter, T. Morphological investigations of single levitated $H_2SO_4/NH_3/H_2O$ aerosol particles during deliquescence/efflorescence experiments. *Journal of Physical Chemistry A* **108**, 2700–2709, DOI: 10.1021/jp037628r (2004).

50. Steimer, S. S. *et al.* Electrodynamic balance measurements of thermodynamic, kinetic, and optical aerosol properties inaccessible to bulk methods. *Atmospheric Measurement*

Techniques **8**, 2397–2408, DOI: 10.5194/amt-8-2397-2015 (2015).

51. Haddrell, A. E., Davies, J. F., Yabushita, A. & Reid, J. P. Accounting for changes in particle charge, dry mass and composition occurring during studies of single levitated particles. *Journal of Physical Chemistry A* **116**, 9941–9953, DOI: 10.1021/jp304920x (2012).

52. Tang, I. N. & Munkelwitz, H. R. Water activities, densities, and refractive indices of aqueous sulfates and sodium nitrate droplets of atmospheric importance. *Journal of Geophysical Research: Atmospheres* **99**, 18801–18808, DOI: 10.1029/94jd01345 (1994).

53. Zardini, A. A. *et al.* A combined particle trap/HTDMA hygroscopicity study of mixed inorganic/organic aerosol particles. *Atmospheric Chemistry and Physics* **8**, 5589–5601, DOI: 10.5194/ACP-8-5589-2008 (2008).

54. Chylek, P. Partial-Wave Resonances and the Ripple Structure in the Mie Normalized Extinction Cross Section. *JOSA* **66**, 285–287, DOI: 10.1364/JOSA.66.000285 (1976).

55. Zardini, A. A., Krieger, U. K. & Marcolli, C. White light Mie resonance spectroscopy used to measure very low vapor pressures of substances in aqueous solution aerosol particles. *Optics Express* **14**, 6951, DOI: 10.1364/OE.14.006951 (2006).

56. Zardini, A. A. & Krieger, U. K. Evaporation kinetics of a non-spherical, levitated aerosol particle using optical resonance spectroscopy for precision sizing. *Optics Express* **17**, 4659–4669, DOI: 10.1364/OE.17.004659 (2009).

57. Zobrist, B. *et al.* Ultra-slow water diffusion in aqueous sucrose glasses. *Physical Chemistry Chemical Physics* **13**, 3514–3526, DOI: 10.1039/c0cp01273d (2011).

58. Bastelberger, S., Krieger, U. K., Luo, B. & Peter, T. Diffusivity measurements of volatile organics in levitated viscous aerosol particles. *Atmospheric Chemistry and Physics* **17**, 8453–8471, DOI: 10.5194/acp-17-8453-2017 (2017).

59. Dou, J. *et al.* Photochemical degradation of iron(iii) citrate/citric acid aerosol quantified with the combination of three complementary experimental techniques and a kinetic process model. *Atmospheric Chemistry and Physics* **21**, 315–338, DOI: 10.5194/acp-21-315-2021 (2021).

60. Carslaw, K. S., Clegg, S. L. & Brimblecombe, P. A Thermodynamic Model of the System HCl-HNO_3-H_2SO_4-H_2O, Including Solubilities of HBr, from <200 to 328 K. *Journal of Physical Chemistry* **99**, 11557–11574, DOI: 10.1021/J100029A039 (1995).

61. Luo, B., Carslaw, K. S., Peter, T. & Clegg, S. L. Vapour pressures of H_2SO_4/HNO_3/HCl/HBr/H_2O solutions to low stratospheric temperatures. *Geophysical Research Letters* **22**, 247–250, DOI: 10.1029/94GL02988 (1995).

62. Bodem, C. R., Lampton, L. M., Miller, D. P., Tarka, E. F. & Everett, E. D. Endobronchial pH: relevance to aminoglycoside activity in gram-negative bacillary pneumonia. *American Review of Respiratory Disease* **127**, 39–41, DOI: 10.1164/arrd.1983.127.1.39 (1983).

63. Choudhury, D. *et al.* Endoscopic sensing of alveolar pH. *Biomed. Opt. Express* **8**, 243–259, DOI: 10.1364/BOE.8.000243 (2017).

64. Holma, B. Effects of inhaled acids on airway mucus and its consequences for health. *Environmental Health Perspectives* **79**, 109–113, DOI: 10.2307/3430536 (1989).

65. Kim, D., Liao, J. & Hanrahan, J. W. The buffer capacity of airway epithelial secretions. *Frontiers in Physiology* **5**, 188, DOI: 10.3389/fphys.2014.00188 (2014).

66. Clegg, S. L., Brimblecombe, P. & Wexler, A. S. Thermodynamic model of the system H^+-NH_4^+-SO_4^{2-}-NO_3-H_2O at tropospheric temperatures. *Journal of Physical Chemistry A* **102**, 2137–2154, DOI: 10.1021/JP973042R (1998).

67. Chan, C. K., Liang, Z., Zheng, J., Clegg, S. L. & Brimblecombe, P. Thermodynamic properties of aqueous aerosols to high supersaturation: I—measurements of water activity of

the system Na^+- Cl^--NO_3^--SO_4^{2-}-H_2O at $\sim$ 298.15 K. *Aerosol Science and Technology* **27**, 324–344, DOI: 10.1080/02786829708965477 (1997).

68. Banerjee, P. & Bagchi, B. Ions' motion in water. *Journal of Chemical Physics* **150**, 190901, DOI: 10.1063/1.5090765 (2019).

69. Staunton, S. Diffusion processes. In Chesworth, W. (ed.) *Encyclopedia of Soil Science*, 185–191, DOI: 10.1007/978-1-4020-3995-9 (Springer Netherlands, 2008).

70. Péraud, J.-P. *et al.* Low mach number fluctuating hydrodynamics for electrolytes. *Phys. Rev. Fluids* **1**, 074103, DOI: 10.1103/PhysRevFluids.1.074103 (2016).

71. Gillespie, D., Nonner, W. & Eisenberg, R. S. Coupling Poisson-Nernst-Planck and density functional theory to calculate ion flux. *Journal of Physics Condensed Matter* **14**, 12129–12145, DOI: 10.1088/0953-8984/14/46/317 (2002).

72. Pruppacher, H. & Klett, J. Microstructure of Atmospheric Clouds and Precipitation. In *Microphysics of Clouds and Precipitation*, 10–73, DOI: 10.1007/978-0-306-48100-0 (Springer, Dordrecht, Dordrecht, 2010), 2 edn.

73. Berry, E. Relative humidity of expired air. *American Physical Education Review* **19**, 452–454, DOI: 10.1080/23267224.1914.10651422 (1914).

74. Berg, H. C. *Random Walks in Biology* (Princeton University Press, Princeton NJ, 1993).

75. Murphy, D. M. & Koop, T. Review of the vapour pressures of ice and supercooled water for atmospheric applications. *Quarterly Journal of the Royal Meteorological Society* **131**, 1539–1565, DOI: 10.1256/qj.04.94 (2005).

76. Nishihama, Y. *et al.* Indoor air quality of 5,000 households and its determinants. Part A: Particulate matter (PM2.5 and PM10–2.5) concentrations in the Japan Environment and Children's Study. *Environmental Research* **198**, 111196, DOI: 10.1016/j.envres.2021.111196 (2021).

77. Seinfeld, J. H. & Pandis, S. N. *Atmospheric chemistry and physics: from air pollution to climate change* (J. Wiley, Hoboken, N.J, 2006), 6th edn.

78. Bourgeois, J. F. & Barja, F. The history of vinegar and of its acetification systems. *Archives des Sciences* **62**, 147–160 (2009).

79. Greatorex, J. S. *et al.* Effectiveness of common household cleaning agents in reducing the viability of human influenza A/H1N1. *PLoS ONE* **5**, e8987, DOI: 10.1371/journal.pone.0008987 (2010).

80. Pagani, I. *et al.* https://www.biorxiv.org/content/10.1101/2020.07.08.193193v2.abstract: Vinegar and Its Active Component Acetic Acid Inhibit SARS-CoV-2 Infection In Vitro and Ex Vivo. *bioRxiv : the preprint server for biology* 2020.07.08.193193, DOI: 10.1101/2020.07.08.193193 (2020).

81. Walker, J. S. *et al.* Accurate representations of the microphysical processes occurring during the transport of exhaled aerosols and droplets. *ACS Central Science* **7**, 200–209, DOI: 10.1021/acscentsci.0c01522 (2021).

82. Ciobanu, V. G., Marcolli, C., Krieger, U. K., Weers, U. & Peter, T. Liquid-liquid Phase separation in mixed organic/inorganic aerosol particles. *Journal of Physical Chemistry A* **113**, 10966–10978, DOI: 10.1021/JP905054D (2009).

83. Kumar, A. *et al.* A biocompatible synthetic lung fluid based on human respiratory tract lining fluid composition. *Pharmaceutical Research* **34**, 2454–2465, DOI: 10.1007/s11095-017-2169-4 (2017).

84. Braun, C. & Krieger, U. K. Two-dimensional angular light-scattering in aqueous NaCl single aerosol particles during deliquescence and efflorescence. *Optics Express* **8**, 314–321, DOI: 10.1364/oe.8.000314 (2001).

85. Bandura, A. V. & Lvov, S. N. The ionization constant of water over wide ranges of temperature and density. *Journal of Physical and Chemical Reference Data* **35**, 15–30,

DOI: 10.1063/1.1928231 (2006).

86. Renard, J. J., Calidonna, S. E. & Henley, M. V. Fate of ammonia in the atmosphere - A review for applicability to hazardous releases. *Journal of Hazardous Materials* **108**, 29–60, DOI: 10.1016/j.jhazmat.2004.01.015 (2004).

87. Sander, R. Compilation of Henry's law constants (version 4.0) for water as solvent. *Atmospheric Chemistry and Physics* **15**, 4399–4981, DOI: 10.5194/acp-15-4399-2015 (2015).

88. Harned, H. S. & Ehlers, R. W. The dissociation constant of acetic acid from 0 to 60° centigrade. *Journal of the American Chemical Society* **55**, 652–656, DOI: 10.1021/ja01329a027 (1933).

89. Morse, J. W. & Mackenzie, F. T. *Geochemistry of Sedimentary Carbonates*, vol. 48 (Amsterdam, 1990).

90. Woosley, R. J. Evaluation of the temperature dependence of dissociation constants for the marine carbon system using pH and certified reference materials. *Marine Chemistry* **229**, 103914, DOI: 10.1016/j.marchem.2020.103914 (2021).

91. Pinho, S. P. & Macedo, E. A. Solubility of NaCl, NaBr, and KCl in water, methanol, ethanol, and their mixed solvents. *Journal of Chemical and Engineering Data* **50**, 29–32, DOI: 10.1021/je049922y (2005).

92. Roberge, P. R. *Corrosion Engineering - Principles and Practice* (McGraw-Hill, 2008).

93. Frank, M. J. W., Kuipers, J. A. M. & Van Swaaij, W. P. M. Diffusion Coefficients and Viscosities of CO_2 + H_2O, CO_2 + CH_3OH, NH_3 + H_2O, and NH_3 + CH_3OH Liquid Mixtures. *Journal of Chemical and Engineering Data* **41**, 297–302 (1996).

94. Kreft, J. U., Picioreanu, C., Wimpenny, J. W. & Van Loosdrecht, M. C. Individual-based modelling of biofilms. *Microbiology* **147**, 2897–2912, DOI: 10.1099/00221287-147-11-2897 (2001).

95. Dryahina, K. *et al.* Exhaled breath concentrations of acetic acid vapour in gastro-esophageal reflux disease. *Journal of Breath Research* **8**, 037109, DOI: 10.1088/1752-7155/8/3/037109 (2014).

96. Smith, D. *et al.* Breath concentration of acetic acid vapour is elevated in patients with cystic fibrosis. *Journal of Breath Research* **10**, 021002, DOI: 10.1088/1752-7155/10/2/021002 (2016).

97. Ejaimi, G. & Saeed, S. An introduction to airway assessment and management (concise airway anatomy and pathophysiology). *Annals of International medical and Dental Research* **3**, 1–7, DOI: 10.21276/aimdr.2017.3.1.an1 (2016).

Acknowledgements

The authors thank Chuck Haas and Mutian Niu for valuable discussions.

Funding

Swiss National Science Foundation grant 189939 (TK, AN, SS, UKK)

Swiss National Science Foundation grant 196729 (TP, UKK)

Author contributions statement

Conceptualization: AN, SS, TK, TP, UKK, WH

Methodology: AS, BL, IG, LKK, MP, NB, SCD, SS, TK, TP, UKK

Investigation: AS, BL, IG, KV, LKK, MP, NB, SCD

Visualization: AS, BL, IG, GM, LKK, KV, SCD, TK, TP

Funding acquisition: AN, SS, TK, TP, UKK, WH

Project administration: TK

Supervision: AN, SS, TK, TP, UKK

Writing–original draft: BL, SS, TK, TP

Writing–review & editing: AN, AS, GM, IG, LKK, MP, NB, SCD, SS, TP, TK, UKK, WH

Competing interests

Authors declare that they have no competing interests.

Data and material availability

Experimental data and ResAM code will be made available upon manuscript acceptance.